



A Comparative Study on Maximum Shear Strain Distribution in a Layered Viscoelastic Medium

Kaveh DEHGHANIAN¹, Mustafa Tolga YILMAZ²

Abstract - For practical calculations, the ovaling and racking deformations on buried structures are estimated by estimating the maximum shear strain (γ_{\max}) in imperforated ground using vertically incident shear waves (V_s). The relationship between maximum shear strain (γ_{\max}) and depth in a uniformly elastic half-space is a function of shear-wave velocity in the uniform medium and acceleration history in free field. In this study, the relationship between the distribution of γ_{\max} in elastic half space and in layered medium is examined by supposing that the travel time of shear waves from the free boundary to a depth of interest in a layered medium is equal to d/V_s . Different variety of strong ground motion time histories and three V_s profiles are used for analyses. The effect of nonlinear material response to shearing was investigated by using the method of equivalent linearization.

Keywords: Shear strain, underground structures, ovaling, racking, free field.

1. Introduction

Underground structures serve as means of transportation, sanitation, irrigation and storage. Recent earthquakes such as Kobe (1995), Kocaeli (1999) and Chi-Chi (1999) showed the vulnerabilities of these structures to severe seismic loads. Ovaling and racking deformations due to vertically induced shear waves are the main causes of seismic damages (Hashash et.al, 2001). Analytical solutions using free field approach and soil-structure interaction have been proposed to calculate ground deformations. In free-field approach, it is assumed that the structure conforms to the surrounding ground deformations. Due to lack of in-situ ground deformation data, simplified formulas are used to calculate γ_{\max} . γ_{\max} is generally related to the formula of Newmark, supposing unidirectional wave propagation in an unbounded uniformly elastic medium, such that

$$\gamma_{\max} = v_{\max} / C \quad (1)$$

where v_{\max} is the maximum particle velocity, and C is the apparent wave velocity (Newmark, 1968; St.John and Zahrah, 1987; Hashash et.al, 2001). For ovaling analyses, a reasonable simplification for computation of γ_{\max} is to assume vertically incident shear waves propagating through horizontal layers (Wang, 1993; Hashash et.al, 2001). In that case, C is approximately equal to V_s , the propagation velocity of shear waves in a layer. However, equation (1) yields conservative estimates for γ_{\max} , especially in shallow ranges of depth. The ground γ_{\max} spectrum provides the

¹ Department of Civil Engineering, Istanbul Aydin University, Istanbul, Turkey, e-mail: kavehdehghanian@aydin.edu.tr

² Department of Engineering Sciences, Middle East Technical University, Ankara, Turkey

relationship between γ_{\max} and depth for an acceleration record on uniformly elastic half space (Chen and Hou, 1992). By defining the seismic hazard in terms of shear-strain spectrum, it is possible to estimate γ_{\max} reasonably for any given depth in a uniformly elastic half space. In order to estimate shear strain in actual sites which generally consists of layered geological formations, a relationship relating γ_{\max} spectra in uniformly elastic half space to the distribution of γ_{\max} in layered soil profiles is necessary. A reasonable method may be the use of equivalent travel-time concept proposed by Imai et al. (1981) for the estimation of maximum shear-stress in layered medium. This is examined for estimation of γ_{\max} in layered soil profiles. Furthermore, the effect of nonlinearity of soil behavior on the accuracy of this method is investigated.

2. Shear-Strain Spectrum

The equation of particle motion due to vertically incident shear waves that propagate with velocity V_s in a linearly elastic medium can be written as

$$\frac{\partial^2 u}{\partial t^2} = V_s^2 \frac{\partial^2 u}{\partial y^2} \quad (2)$$

where, $u(t,y)$ depicts the horizontal displacement of a particle located at coordinate y and at time t due to the disturbance propagating in the vertical direction. The relationship between shear strain (γ) at any depth (d) and shear wave velocity is

$$V_s \cdot \gamma^F(\omega, d/V_s) = \frac{a^F(\omega)}{\omega} \cdot \sin\left(\frac{\omega}{V_s} d\right) \quad (3)$$

In equation (3), a^F denotes the complex Fourier coefficient of acceleration history (a) in free field. Equation (3) can be expressed in time domain by

$$V_s \cdot \gamma(t, d/V_s) = \frac{1}{2} [v(t + d/V_s) - v(t - d/V_s)] \quad (4)$$

where $v(t)$ is the velocity history in free field. Hence, γ_{\max} is a function of d/V_s , the travel time of vertically incident shear waves from free boundary to a point at depth d (Chen and Hou, 1992).

3. The Concept of Equivalency in Travel Time

Equations (3) and (4) are applicable for uniformly elastic half space. According to Imai et al. (1981), the maximum shear stress (τ_{\max}) at any given depth in layered soils can be estimated by supposing that the travel time of vertically incident shear waves from the free boundary to the depth of interest is equivalent to the travel time in a hypothetically uniform elastic medium. This travel time is calculated by the formula,

$$\frac{d}{V_s} = \sum_{i=1}^l \frac{d_i}{V_i} \quad (5)$$

for the estimation of τ_{\max} in the l^{th} layer below the ground surface. Then, γ_{\max} can be calculated by

$$\gamma_{max} = \frac{\tau_{max}}{\rho_l \times (V_s)_l^2} \quad (6)$$

where ρ_l and $(V_s)_l$ are respectively the density and the shear-wave velocity of the layer of interest. Hence, d/V_s calculated by equation (5) is first substituted in equations (3) or (4) for the estimation of $V_s\gamma(t)$. Then, by supposing that $V_s = (V_s)_l$, the maximum absolute value of $V_s\gamma(t)$ yields γ_{max} for the l^{th} layer. The procedure can be simplified if the relationship between d/V_s and $V_s\gamma_{max}$ is first computed for any given $a(t)$, and then d/V_s calculated by equation (5), is used for interpolation in the calculated range of $V_s\gamma_{max}$.

Equations (3) to (5) are based on the assumption of linearly elastic medium whereas the geological formations are expected to show nonlinear stress-strain response to severe shearing during seismic events. The effect of nonlinear material behavior on γ_{max} can be involved in calculations by the well-known method of equivalent linearization (Schnabel et al., 1972). The accuracy of the method was investigated by the comparisons with the 1-dimensional site-response analyses. The program PROSHAKE, computing the dynamic site response by the method of equivalent linearization (EduPro Civil Systems, 1998), was used for the determination of γ_{max} in each layer. In the analyses, the ground motion was defined for a hypothetical station on the ground surface, so that $\gamma(t)$ was computed by the deconvolution technique. The strain-dependent degradation in shear modulus (G), and the increase in material damping (ξ) were modeled by the empirical relationship of Vucetic and Dobry (1991), applicable to lightly over-consolidated fine soils with a Plasticity Index of 15, so that the strain-dependent reduction in material rigidity is significant in the dynamic response analyses. The representative value for ξ and the reduction in G are estimated by supposing that the cyclic amplitude of γ is equal to 65% of γ_{max} . $(V_s)_l$ is proportional to the square-root of G in the equivalent-linear method of analysis due to the relation $G = \rho \times (V_s)$. The tolerable relative error, the limit for relative difference between the results of successive iterations, was accepted as 1%. In these analyses, the secant shear modulus is changed for each layer until their values are consistent with γ_{max} induced in each layer. The same iterative procedure was implemented in a spread sheet program for the calculation of γ_{max} by the shear-strain spectrum.

4. Analyses

A number of accelerograms were selected from the strong-motion databases PEER and DAPHNE to collect a sample for the empirical determination of parameters. The emphasis was placed on using the records that involve significant ground-motion amplitudes for buried structures. The PEER database provided filtered records. The records are attributed to the seismic events presented in Table 1. The sites of records were classified according to the site classification system of *International Building Code* (ICC, 2009). This widely known system is related to the parameter V_{s30} , the weighted harmonic mean of V_s to the depth of 30 m (Borcherdt, 1994). The site class D is pertinent to stiff-soil ($180 \text{ m/s} \leq V_{s30} \leq 360 \text{ m/s}$) condition. The frequencies above 15 Hz can be heavily contaminated for accelerograms by high-frequency surface waves and by waves reflected from stratified formations. The high-frequency contamination yields amplitudes that are not consistent with the assumptions about the properties of viscoelastic media considered in analyses, and can be suppressed by a low-pass filter to improve the coherence between the velocity profiles and the accelerogram defining the free-field motion (Silva, 1988). Therefore, the records were filtered by a 4-pole/4-pole low-pass Butterworth filter (Akkar and Bommer, 2007). The ground motion records presented in Table 1 were supposed to be the records of ground motion in free field after suppressing the frequencies above 15 Hz.

Three real velocity profiles, shown in Figure 1, were considered in site-response analyses. The first profile (Figure 1.a) is adopted from the site *Bell-La Bulk Mail* presented by Nigbor and Swift (2001). The second and third profiles (1.b, and 1.c) are adopted from the sites *Gilroy #2 (USGS)* and *Palo Alto Veterans Hospital* presented by Boore et al. (2003). An elastic half space representing the soft rock was considered to be lying beneath the viscoelastic layers. The distribution of V_s with respect to d/V_s in three sites is shown in Figure 2. d was taken as the average depth of each uniformly viscoelastic layer. The material density of all actual formations was set to 2000 kg/m^3 , so that the results of analyses can be solely attributed to the distribution of V_s .

The records 6 and 16 (Table 1) were scaled by the factor 0.60 to keep γ_{\max} below 1% because the accuracy of equivalent linearization in site-response analysis can be considerably low if γ_{\max} is greater than 1% (Gerolymos and Gazetas, 2005). Due to the size limitations in the computer program, the record numbered as 20 in Table 1 was cropped to shorten the record length by the 70 seconds that involve the most significant amplitudes of ground motion. The cropped record was filtered at high-pass frequency of 0.1 Hz.

Table 1: The list of ground-motion records.

Rec. No.	Event No.	Station	Vs30	SC	Event Name	Event Date	Ms	Depth (km)
1	1	Gormon - Oso Pump Plant	308	D	San Fernando	9.02.1971	6.6	13.0
2	2	Capitola	288	D	Loma Prieta	18.10.1989	7.1	17.5
3	2	Gilroy Array #2	270	D	Loma Prieta	18.10.1989	7.1	17.5
4	2	Gilroy Array #3	349	D	Loma Prieta	18.10.1989	7.1	17.5
5	2	Gilroy - Historic Bldg.	338	D	Loma Prieta	18.10.1989	7.1	17.5
6	3	Eureka - Myrtle & West	338	D	Cape Mendocino	25.04.1992	7.1	9.6
7	4	Amboy	271	D	Landers	28.06.1992	7.4	7.0
8	4	Fort Irwin	345	D	Landers	28.06.1992	7.4	7.0
9	4	Hemet Fire Station	338	D	Landers	28.06.1992	7.4	7.0
10	5	Inglewood - Union Oil	316	D	Northridge	17.01.1994	6.7	17.5
11	5	LA - Century City CC North	278	D	Northridge	17.01.1994	6.7	17.5
12	5	LA - E Vernon Ave	308	D	Northridge	17.01.1994	6.7	17.5
13	6	KJMA	312	D	Kobe	16.01.1995	6.9	17.9
14	6	Kakogawa	312	D	Kobe	16.01.1995	6.9	17.9
15	6	Takarazuka	312	D	Kobe	16.01.1995	6.9	17.9
16	6	Takatori	256	D	Kobe	16.01.1995	6.9	17.9
17	6	Shin-Osaka	256	D	Kobe	16.01.1995	6.9	17.9
18	7	1612	197	D	Kocaeli	17.08.1999	7.7	15.9
19	7	5903	325	D	Kocaeli	17.08.1999	7.7	15.9
20	8	CHY036	233	D	Chi-chi	20.09.1999	7.6	6.8

SC: site class (International Code Council).

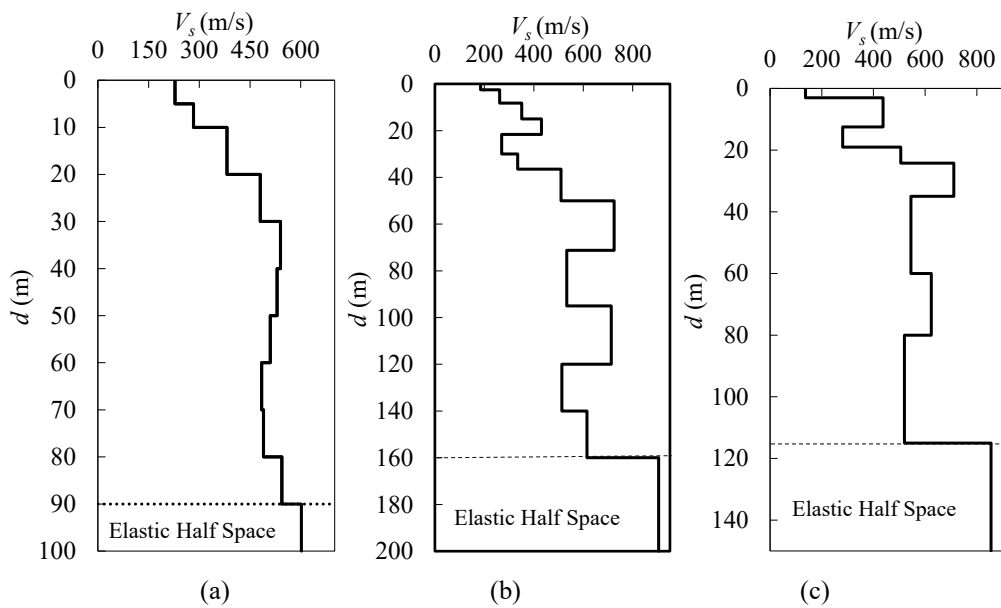


Figure 1: Velocity profile used for the site response analyses for (a) *Bell - La Bulk Mail* site, for (b) *Gilroy #2 (USGS)*, and for (c) *Palo Alto Veterans Hospital*.

Figure 3 shows the range of geometric means of maximum strain ratio ($\gamma_{\max-l}/\gamma_{\max}$) for two horizontal components of ground motion used in PROSHAKE analyses, such that a linear relationship between stress and strain is considered. $\gamma_{\max-l}$ denotes maximum absolute shear strain computed by PROSHAKE. $V_s \gamma_{\max}$ is calculated by equation (3) or (4). Then, γ_{\max} is calculated by supposing that $V_s = (V_s)_l$. The comparisons of figures (2) and (3) reveal that this analysis is very sensitive to the variability in V_s . An investigation of the ratio between V_s in soft layers and that in stiffer layers shows that the method may slightly underestimate γ_{\max} in soft layers located beneath much stiffer layers. However, the predictions are conservative for most of the layers. For instance, the lowest V_s ratio (0.62) occurs at the travel time 0.07 s at the site *Gilroy #2 (USGS)*, such that $\gamma_{\max-l}/\gamma_{\max}$ is 1.16. In contrast, at the site *Bell - La Bulk Mail site*, the V_s ratio is the highest (0.94) for $d/V_s = 0.14$ s, but $\gamma_{\max-l}/\gamma_{\max}$ is almost 1.0. Whereas, at the site *Palo Alto Veterans Hospital* the V_s ratio is considerably low (0.64) for $d/V_s = 0.05$ s, which is close to the minimum ratio at the site *Gilroy #2 (USGS)*, but the underestimation of γ_{\max} is negligible. One important observation is that, the scattering of $\gamma_{\max-l}/\gamma_{\max}$ for any given d/V_s is very limited.

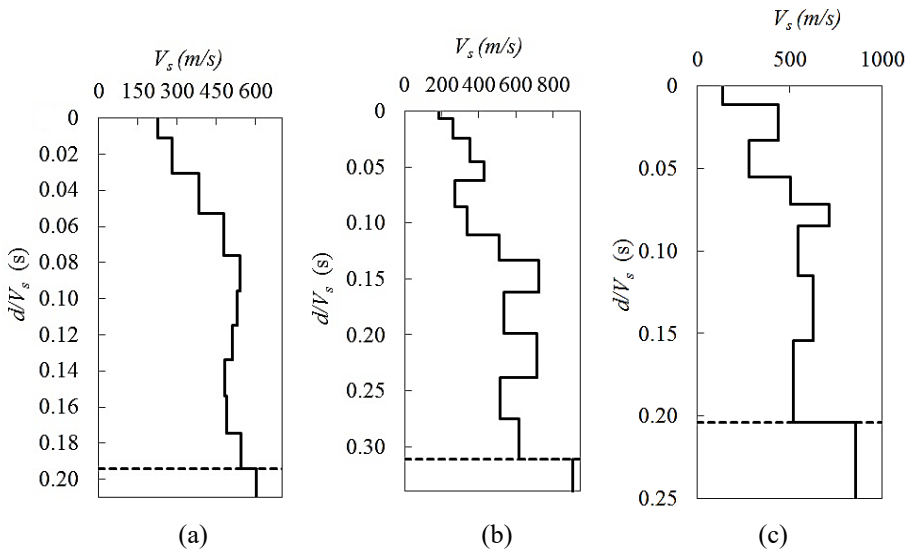


Figure 2: The travel times for middle geological layers on the sites (a) *Bell - La Bulk Mail*, (b) *Gilroy #2 (USGS)*, and (c) *Palo Alto Veterans Hospital*.

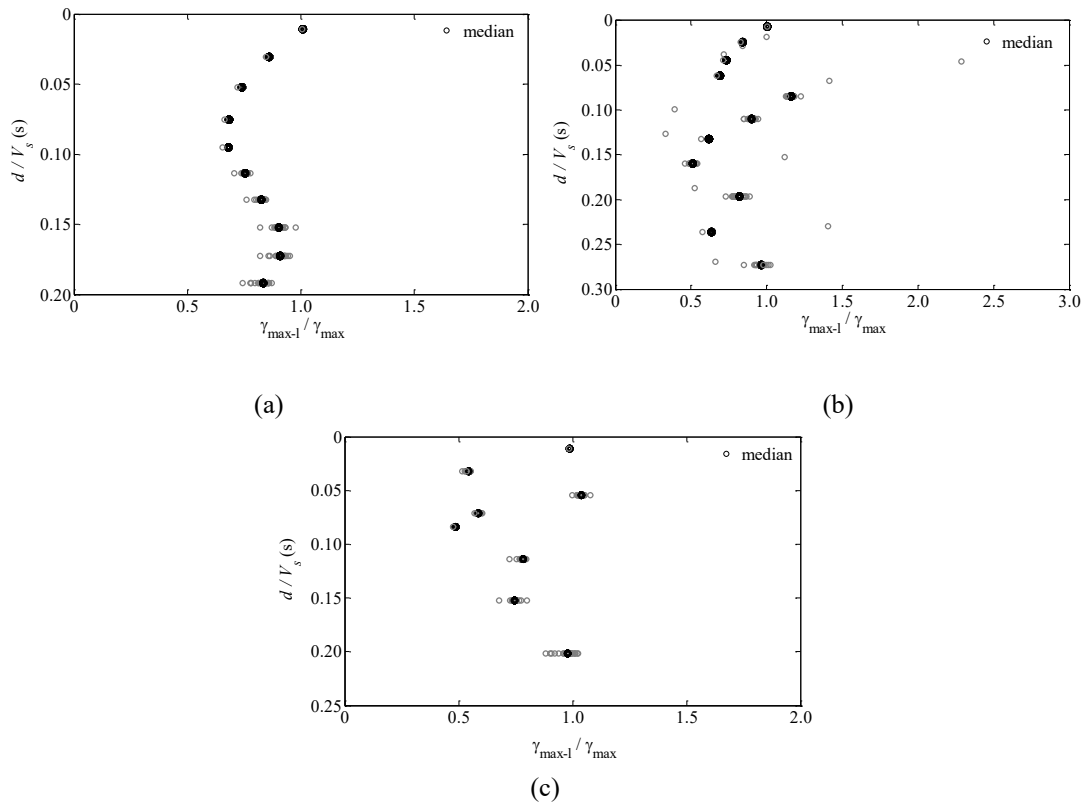


Figure 3: The ranges of $\gamma_{\max-l}/\gamma_{\max}$ computed by supposing linear response of layers on the sites (a) *Bell - La Bulk Mail*, (b) *Gilroy #2 (USGS)*, and (c) *Palo Alto Veterans Hospital*.

In order to investigate the effect of nonlinearity of soils' response to shearing, the same profiles were analyzed by using the relationships between ξ_s (G/G_{\max}) and cyclic amplitude of γ that were suggested by Vucetic and Dobry (1991). Figure 4 shows the scattering of $\gamma_{\max-l}/\gamma_{\max}$ by d/V_s . The comparisons of figures (3) and (4) reveals that the scattering of $\gamma_{\max-l}/\gamma_{\max}$ and the underestimation of equation (3) for embedded soft layers can be more prominent if the soils behave nonlinearly. This can be explained by the reduction in G , consequently in equivalent V_s . Except for these soft layers embedded in much stiffer layers, equation (3) usually yields a reasonable or conservative estimate for γ_{\max} .

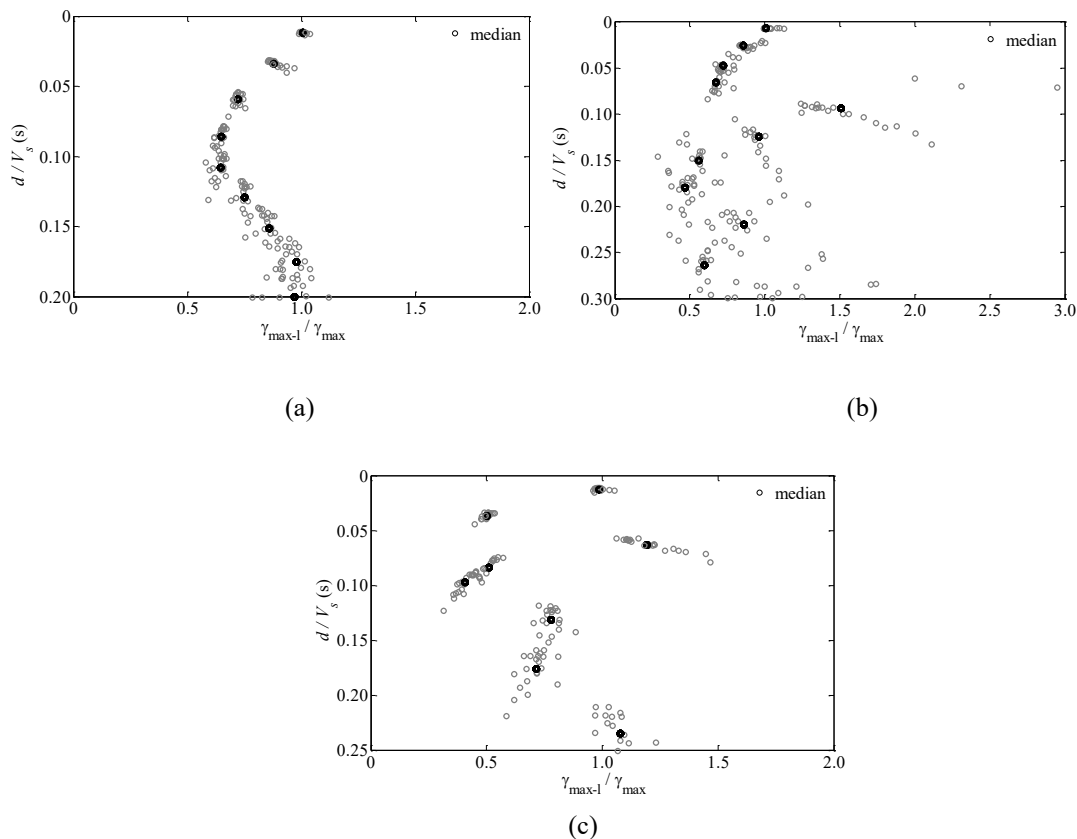


Figure 4: The ranges of $\gamma_{\max-l}/\gamma_{\max}$ computed by supposing nonlinear response of layers on the sites (a) *Bell - La Bulk Mail*, (b) *Gilroy #2 (USGS)*, and (c) *Palo Alto Veterans Hospital*.

6. Conclusions

The assumption that the parameter $V_s\gamma_{\max}$ in any soil layer is strongly related to the travel time of shear waves from ground surface to the depth of interest yields a method for the estimation of γ_{\max} , provided that the shear-strain spectrum suggested by Chen and Hou (1992) is available. Therefore, in calculation of seismic hazard for buried structures and in the selection of ground-motion records, the emphasis should be given to this spectrum. However, strain ratio is sensitive to the site layering, and may show limited scattering. The procedure explained in this study may result in the underestimation of γ_{\max} in soft layers embedded in much stiffer layers. Detailed site-response analyses for the calculation of γ_{\max} in such soft layers are observed to be crucial. Otherwise, the method yields either reasonably accurate or conservative estimates for γ_{\max} in layered geological formations. The accuracy of the method is very satisfactory for almost uniform V_s profiles. All conclusions are based on the assumption that the ground motion is

induced by a field of vertically propagating shear waves. Hence, the proposed method can be acceptable for first-order estimations of γ_{\max} , particularly in the absence of the data necessary for more accurate analysis methods, if the seismic hazard is expressed by a shear-strain spectrum.

References

- [1] Akkar, S. and Bommer, J. (2007). Empirical Prediction Equations for Peak Ground Velocity Derived from Strong-Motion Records from Europe and the Middle East, *Bulletin of the Seismological Society of America*, Vol. 97, No. 2, pp. 511–530.
- [2] Borcherdt, RD. (1994). Estimates of Site-Dependent Response Spectra for Design (Methodology and Justification). *Earthquake Spectra*, Vol.10, No.4, pp. 617-653.
- [3] Boore, D.M., Gibbs, F. and Rodriguez, M. (2003). *A compendium of P- and S-wave velocities from surface-to-borehole logging; summary and reanalysis of previously published data and analysis of unpublished data*. Open-File Report 2003-191, USGS, California, United States of America.
- [4] Chen, CH. and Hou, PC. (1992). Response Spectrum of Ground Shear Strain. *10th World Conference on Earthquake Engineering*, Rotterdam.
- [5] Daphne, Strong Ground Motion Database of Turkey. (15 May 2014). http://daphne.deprem.gov.tr/2K/daphne_v4.php.
- [6] ICC, International Code Council. (2009). *International Building Code*, the United States.
- [7] EduPro Civil Systems. (1998). *PROSHAKE – Ground Response Analysis Program*, EduPro Civil Systems Inc., Redmond, Washington.
- [8] Gerolymos, N. and Gazetas G. (2005). Constitutive Model for 1-D Cyclic Soil Behavior Applied to Seismic Analysis. *Soils and Foundations*, Vol. 45, No.3, pp. 147-159.
- [9] Hashash, YMA, Hook, JJ, Schmidt, B and Yao JIC. (2001). Seismic Design and Analysis of Underground Structures. *Tunneling and Underground Space Technology*, Vol.16, No.4, pp.247–293.
- [10] Imai T, Tonouchi K. and Kanemori T. (1981). *The Simple Evaluation Method of Shear Stress Generated by Earthquakes in Soil Ground*. Bureau of Practical Geological Investigation: Japan, pp. 39-58.
- [11] Newmark, NM. (1968). *Problems in Wave Propagation in Soil and Rock*. Symposium on Wave Propagation and Dynamic Properties of Earth Materials, August 23-25, Univ. of New Mexico Press, Albuquerque, NM, pp. 7-26.
- [12] Nigbor, R.L. and Swift J.N. (2001). *Resolution of Site Response Issues from the Northridge Earthquake*, ROSRINE/ USC-01, Revision 0.9, 26 November.
- [13] PEER Strong Ground Motion Database. (15 May 2014). <http://peer.berkeley.edu/smcat/>.
- [14] Schnabel, PB, Lysmer, J. and Seed, HB. (1972). *SHAKE: A Computer Program for Earthquake Response Analysis of Horizontally Layered Sites*. Report No. UCB/EERC-72/12, Earthquake Engineering Research Center, University of California, Berkeley, pp. 1-92.
- [15] Silva, W. (1988). *Soil Response to Earthquake Ground Motion*, EPRI NP-5747 Final Report, Woodward-Clyde Consultants, California.
- [16] St. John, CM. and Zahrah, TF. (1987). Aseismic Design of Underground Structures. *Tunneling and Underground Space Technology*, Vol. 2, No. 2, pp. 165 -197.
- [17] Vucetic, M. and Dobry, R. (1991). Effect of Soil Plasticity on Cyclic Response. *Journal of Geotechnical Engineering*, Vol.117, No.1, pp. 89-107.
- [18] Wang, JN. (1993). *Seismic Design of Tunnels, a Simple State-of-the-Art Design Approach*. Parsons Brinckerhoff Inc. Publication, New York, pp. 53-133.



Structural Performance Assessment of Historical Dilovasi Sultan Suleyman (Diliskelesi) Bridge in Turkey

Ferit CAKIR

Abstract - Masonry arch bridges are regarded as the oldest examples of engineered structures in the world and they reflect the culture of previous civilizations with their various sizes, styles, and spans. These bridges were constructed centuries ago addressing the load-carrying problems of old times. The preservation of these structures receives a great deal of attention in the structural engineering community. In this respect, current study focuses on historical Dilovası Sultan Suleyman (Diliskelesi) Bridge in Kocaeli, Turkey. In order to investigate the structural behavior of the current form of the bridge, Modal and Response Spectrum analyses were carried out utilizing finite element methods.

Keywords: *Masonry arch bridges, Dilovası Sultan Suleyman (Diliskelesi) Bridge, Modal Analysis, Response Spectrum Analysis, Finite Element Method*

1. Introduction

Many masonry bridges have been built in earthquake prone regions of the world and a large portion of them are not seismically safe. Historical arch bridges, encompassing various sizes, styles, and spans reflect the cultures of the previous civilizations. As such, they constitute an important part of the cultural heritage in the world, hence their preservation for the next generation is crucial. Indeed, several of these structures which are over 2000 years old, are already vital components of transportation systems in many communities (Sevim et al. 2011). As a consequence of the long history of arch bridges, many samples exist around the world. Figure 1 provides a typical detail of various components making up a masonry arch bridge. Individual components have their own names that are universally accepted as the terminologies used to identify these components. An essential understanding of the structural behavior of masonry arch bridges requires information about their structural elements.

¹ Associate Prof., Department of Civil Engineering, Istanbul Aydin University, Istanbul, Turkey. e.mail: feritcakir@aydin.edu.tr

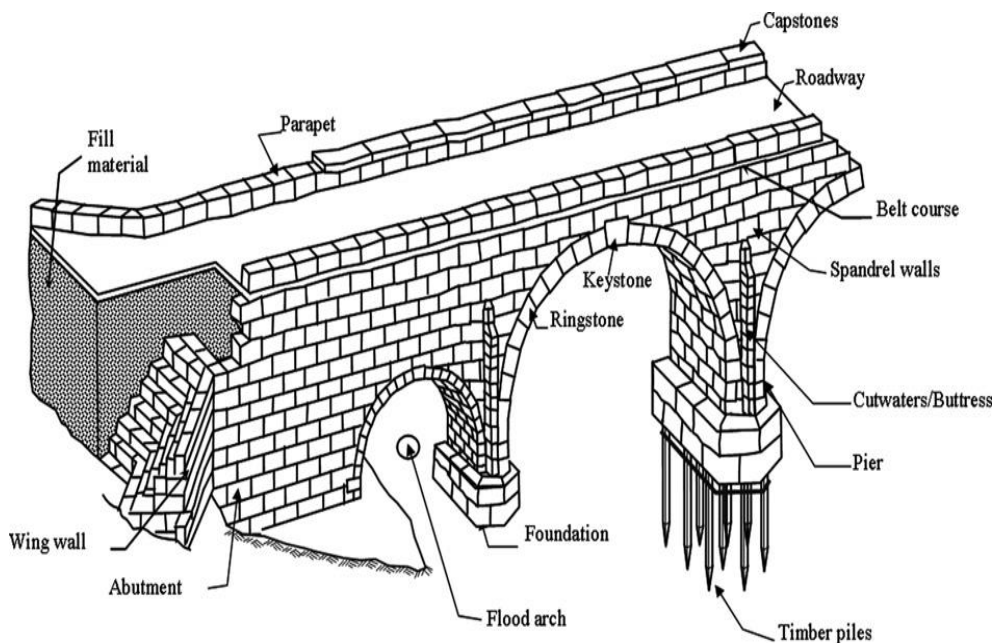


Figure 1: Main components of a masonry arch bridge (Ural et al. 2008)

2. Seismic Behavior of Masonry Bridges

Masonry arch bridges are exposed to many different external and internal effects throughout their lives. An understanding of the load carrying capabilities of these bridges and an estimation of the type and intensity of load on them would be beneficial in order to better understand the performance of these bridges and how they have been able to survive the changes in the loading regime. The fact that many masonry bridges have been able to keep up with these loads and changes is a testimony to the complexity of their structural behaviors. Major loads on masonry bridges are dead loads, live loads, lateral loads, and water and earth forces. Lateral loads are horizontal loads acting on the structures and might be the most dangerous loads for masonry bridges. The most common lateral load is due to earthquake which has a dynamic nature. An earthquake load is a function of the mass of the structure and the intensity of the ground acceleration. Since the nature of earthquakes is random, the timing of the occurrence and the magnitude of the corresponding loads due to earthquake is uncertain. Therefore, the potential damaging effects of earthquakes may become more severe than those of the wind loads. Masonry bridges have large masses due to heavy construction materials such as stones, bricks and mortars. Thus, earthquake load significantly affects masonry bridges. The heavy mass increases the intensity of the force on the bridge. At the same time, the ancient masonry structures lack the structural ductility that is needed to perform well during earthquakes. As a result, the masonry bridges are vulnerable to earthquakes and seismic effects have been among the most important reasons for collapse among masonry bridges. Earthquake loads originate from ground shaking and formation of seismic waves which usually have two major components -- horizontal and vertical. Recent research shows that the horizontal waves are more dangerous than the vertical waves on masonry structures; and many ancient and newer masonry structures have been destroyed due to horizontal waves (Meyer, 2006). According to the reports on earthquake damages on masonry bridges, earthquake damages are observed in the spandrels (Figure 2) or the superstructures (Figure 3) (Cakir and Seker, 2015; Cakir, 2011).



Figure 2: Collapse of spandrel of a masonry bridge during the 1997 Umbria-Marche earthquake



Figure 3: Damages occurred in superstructure of the Misis Bridge during the 1998 Adana-Ceyhan earthquake (Ural et al. 2008)

3. Historical Dilovası Sultan Suleyman (Diliskelesi) Bridge in Kocaeli

Kocaeli is one of the oldest settlements of Anatolia, which is located in the Marmara Region in Turkey. Established at the intersection of a major road and rail routes between Asia and Europe, Kocaeli is one of the most important industrial sites in the Marmara Region today (Figure 4). The history of Kocaeli dates back to much older times. In the early ages, the region was called Bithynia and different cities were established in the region throughout the history named Olbia, Astakos, Nicomedia, Iznikmid, Izmit and Kocaeli respectively. Due to its historical background, Kocaeli is primarily a cultural destination; it has a rich cultural heritage. One of the well-known historical structures in the region is Dilovası Sultan Suleyman (Diliskelesi) Bridge. Since the bridge is located in socially and culturally active areas, it is intensely used in the present day.



Figure 4: Map of Turkey (Adapted from Google Maps)

Dilovası Sultan Suleyman (Diliskelesi) Bridge, ordered by Kanuni Sultan Süleyman and built by Architect Sinan in the 16th century, is 45 meters long. The structure is located on a creek with the same name in the Dilovası district of Kocaeli. The bridge has a small evacuation eye at the end of the middle belt opening which is 10.60 meters. The relatively smaller arches on both sides of the large arch in the middle are made of limestone cut in sharp forms (Kantaratlas, 2018). The keystone of the belt is placed outwardly (Figure 5).

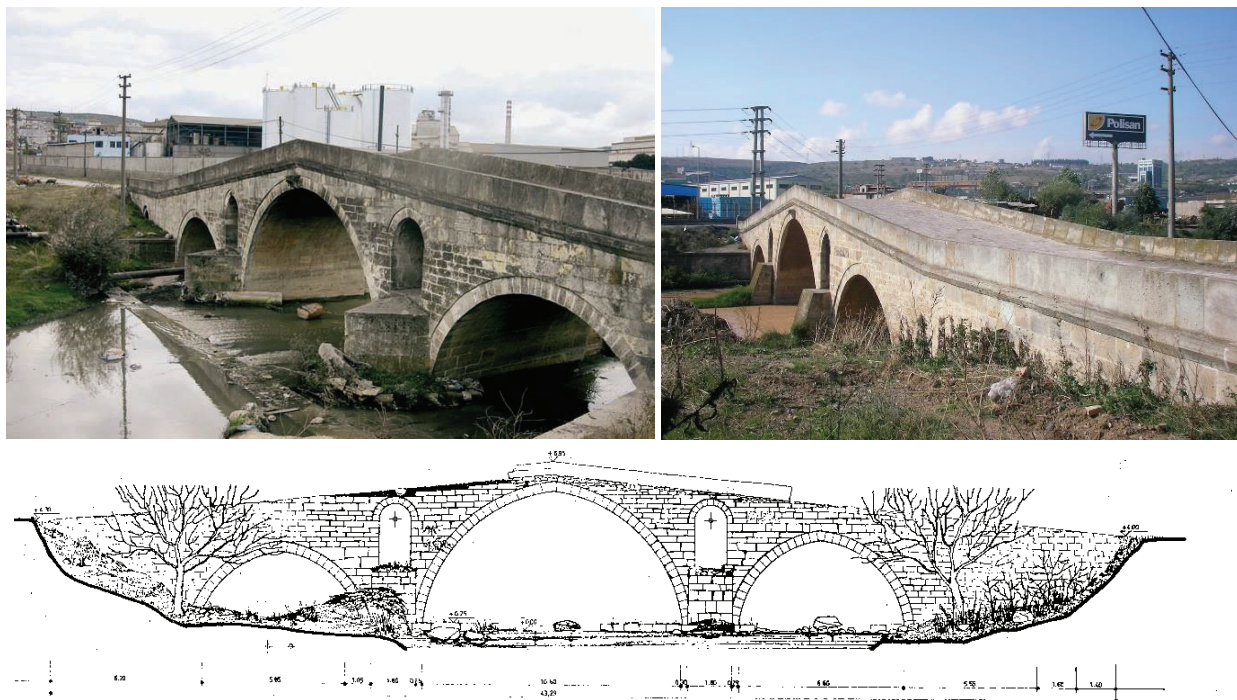


Figure 5: Dilovası Sultan Suleyman (Diliskelesi) Bridge (Kantaratlas, 2018; Şükür, 2008)

4. Structural Performance Assessment of historical Dilovası Sultan Suleyman (Diliskelesi) Bridge

In this study, firstly, the numerical model was prepared using finite element analysis (FEA) program, ANSYS Workbench (2017). In the modeling process, SOLID 65 elements, which have eight nodes and three degrees of freedom per node, was preferred for the description of the bridge. The three-dimensional model was discretized with 317025 nodes and 188775 solid elements (Figure 6). Modal Analysis and Response Spectrum Analysis (RSA) were performed on the numerical model. The obtained analyses results were too complicated to present each node or element, therefore, contour pictures, bars, and scale tables were used to present the results of the analyses. Moreover, fixed boundary conditions were considered in the foundation sections and sidewalls. The mechanical properties used in all numerical analyses are summarized in Table 1 (Cakir and Seker, 2015; Cakir and Uysal, 2014; Cakir et al, 2014).

Table 1: Mechanical properties of the materials

Component of Structure	Young Modulus (MPa)	Poisson's Ratios	Density (kg/m3)
Arches	10000	0.25	2500
Spandrel	8500	0.25	1850

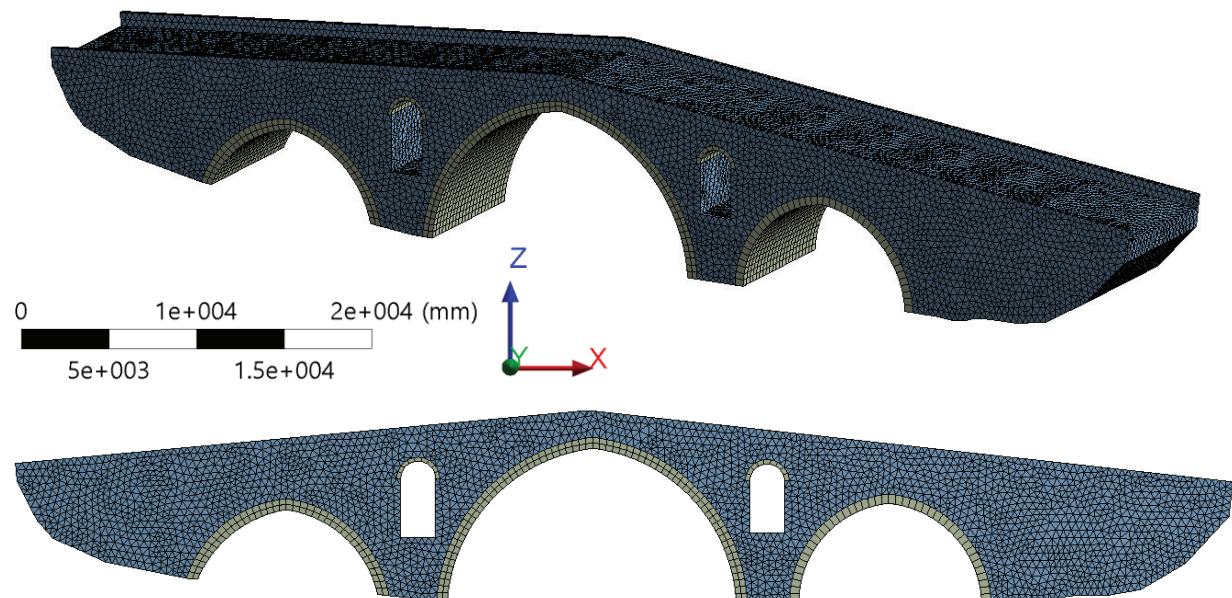
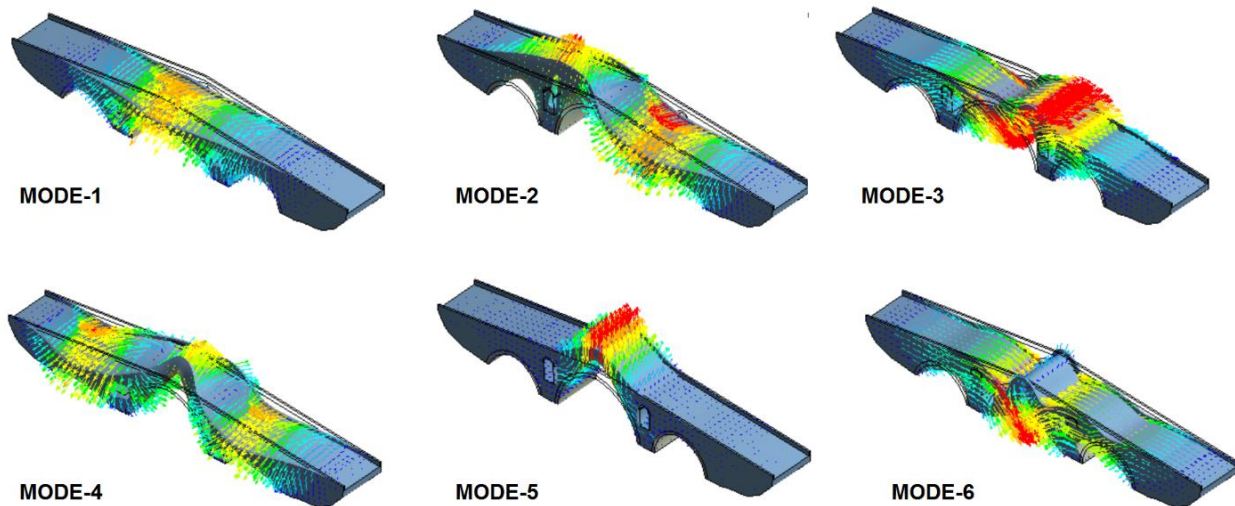


Figure 6: Numerical model of the bridge

The modal analysis of vibration is simply used to determine mode shapes and characterizing resonant frequencies. Modal analysis changes from a multiple degree of freedom problem to a vibration problem. In the dynamic analysis of the bridge, primarily mode shapes and mode vibration periods were determined; the first four mode frequencies, periods, and mass participation ratios were summarized in Table 2. Furthermore, the first six mode shapes were shown in Figure 7.

Table 2: The first six mode frequencies, periods, and mass participation ratios

Mode	Frequency (Hz)	Period (s)	Ratio Eff. Mass To Total Mass X Direction	Ratio Eff. Mass To Total Mass Y Direction	Ratio Eff. Mass To Total Mass Z Direction
1	21.1240	0.47340E-01	0.116013E-08	0.327952	0.281701E-08
2	29.7189	0.33649E-01	0.143925E-08	0.138867E-02	0.388626E-09
3	31.7833	0.31463E-01	0.429338	0.123221E-08	0.846705E-04
4	36.8151	0.27163E-01	0.146073E-10	0.210250	0.259064E-06
5	37.7064	0.26521E-01	0.200814E-03	0.404817E-06	0.967770E-01
6	47.1976	0.21188E-01	0.244307E-02	0.330740E-10	0.877093E-01

**Figure 7:** The first six mode shapes

The seismic performance of the bridge was also investigated through RSA conducted on the finite element model in horizontal direction. The response spectrum corresponding to the seismic hazard level was selected by using Turkey's New Earthquake Hazard Map (Figure 8). The simulated ground records for the 475 year return period (the possibility to be exceeded in 50 years is 10%) were used in the evaluation of the bridge.

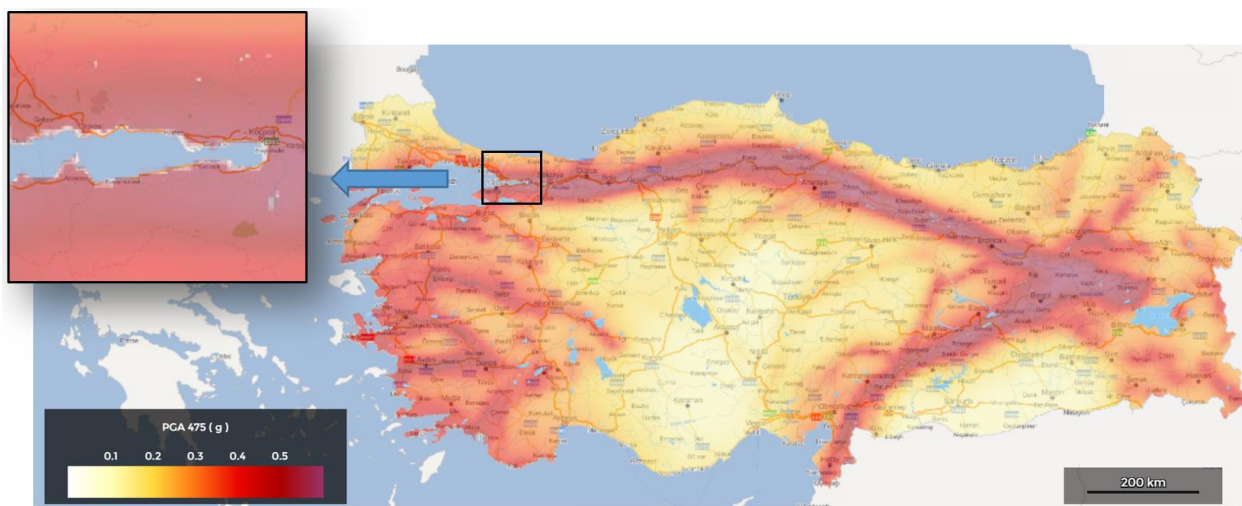


Figure 8: Earthquake Regions Map of Turkey and Kocaeli

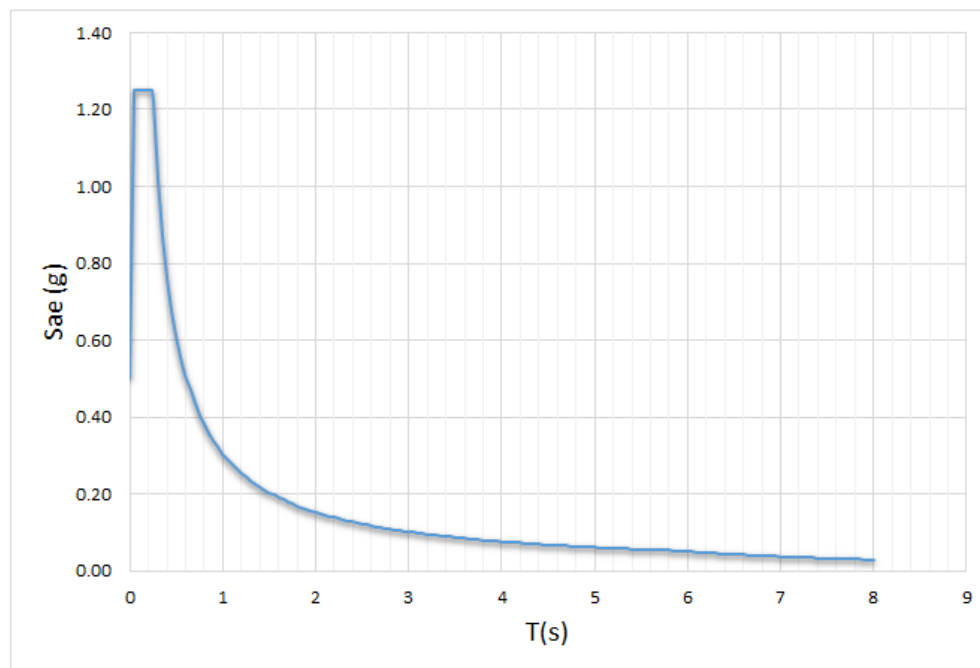


Figure 9: Uniform hazard spectra for the selected seismic hazard level.

The maximum normal stress was found to be 3.6997 MPa around the base section of the small arch of the bridge (Figure 10). The obtained equivalent stress was about 3.0595 MPa around the bridge base (Figure 11). Moreover, the observed maximum lateral displacement was about 1.4514mm at the top of the bridge corresponding to 0.02% drift ratio (Figure 12). Table 3 indicates that at this drift ratio level, the structural response of the bridge is below the immediate occupancy (IO) damage level (0.1%). In the light of the obtained information, it is seen that the structure is quite good in terms of earthquake performance.

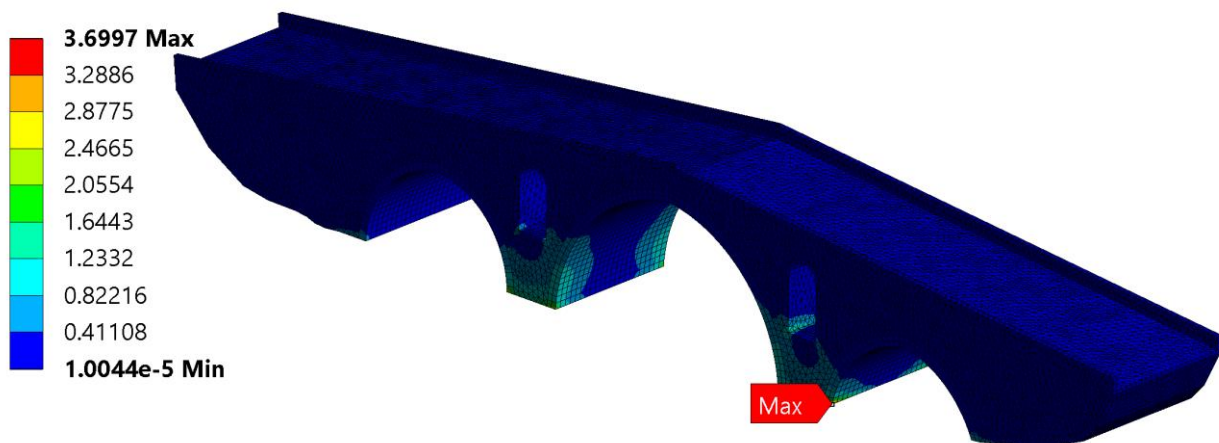


Figure 10: Normal stress obtained from the RSA

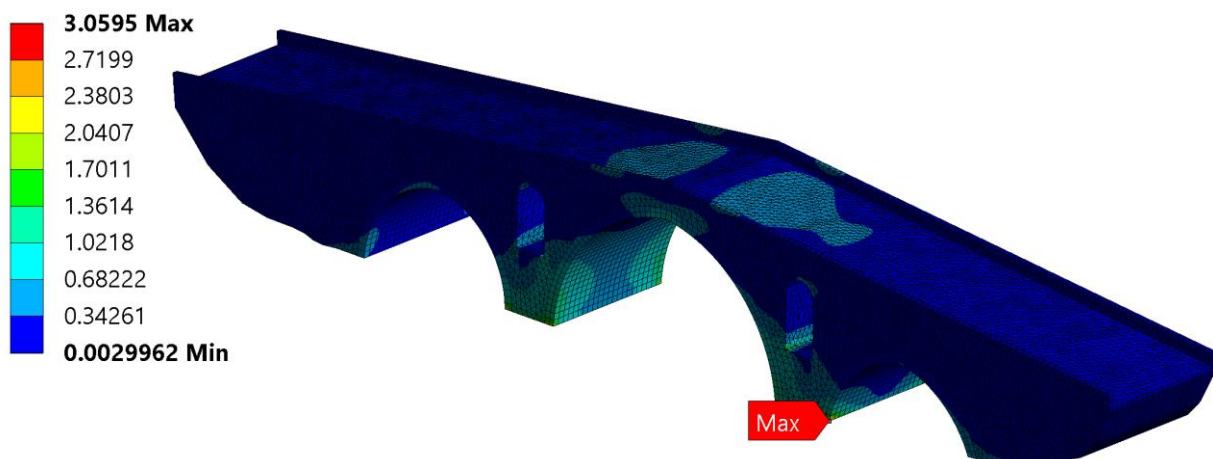


Figure 11: Equivalent stress obtained from the RSA

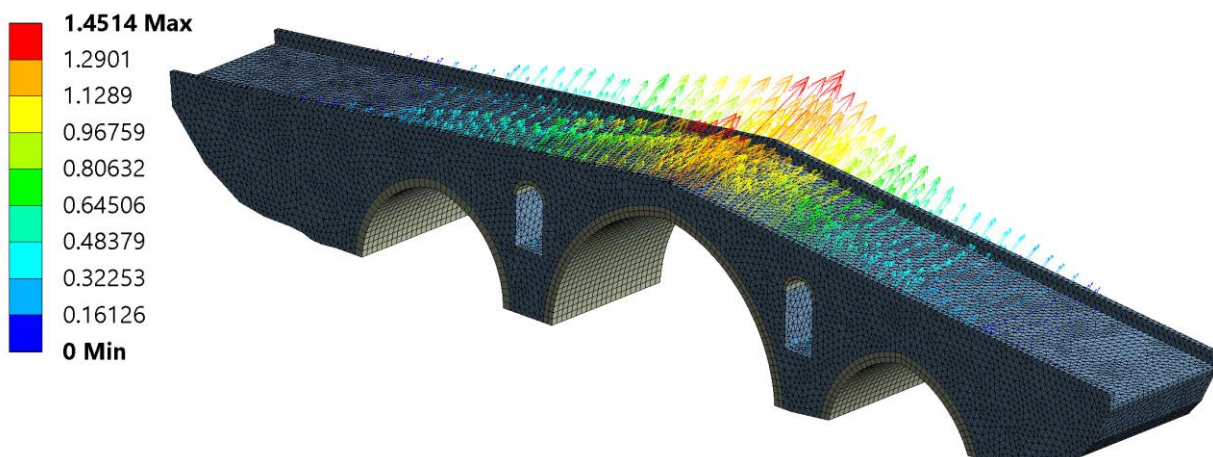


Figure 12: Maximum lateral displacement obtained from the RSA

Table 3: Acceptance criteria for unreinforced masonry in-plane walls and piers

Limiting behavioral node	Primary members			Secondary members	
	Immediate occupancy (IO) (%)	Life safety (LS) (%)			
FEMA 356	Bed-joint sliding	0.1	0.3	0.4	0.6
FEMA 274	Rocking	0.1	$0.3h_{eff}/L$	$0.4h_{eff}/L$	$0.6h_{eff}/L$
ASCE 41	Rocking	0.1	$0.3h_{eff}/L$	$0.4h_{eff}/L$	$0.6h_{eff}/L$

5. Conclusions

Historical structures that are built centuries ago reflect the previous civilizations which have passed the world. Today, it is still possible to see some of these structures as a whole. These magnificent structures need to be well protected and preserved due to their historical and cultural values. Many historical structures are located at earthquake prone zones in the world, and the majority of these structures are considered to be seismically inadequate and unsafe. Historical bridges face many inadequacies in terms of seismic performance. Thus, they have to be retrofitted with the convenient restoration methods against earthquake damages. To determine the structural protection requirements for these structures, a deep understanding of their behavior and an effective evaluation of the structural integrity and failure mechanism is needed. The subject of earthquake hazard assessment of a historical structure has gained great attention in the last few decades. A sustained effort on the subject is strongly needed.

This paper briefly investigates the basic principles to be considered in performance-based seismic evaluation of historical structures. The seismic performance evaluation of the historical Sultan Suleyman (Diliskelesi) Bridge in Kocaeli, Turkey is presented. RSA was used for the performance evaluation. The seismic hazard levels, evaluation of existing seismic hazard, selection of earthquake ground motions as well as site geology, geological and tectonic settings of the area, seismic activity of the region and local soil conditions are needed for a thorough evaluation. The results of the analyses show that the critical stresses are calculated in the base section of the bridge and arch. It is also detected that the supports of the arches that carry the spandrel of the bridge deserve special attention since they have a considerable effect in the structural performance.

References

- [1] ANSYS, (2017). 18.2 Release, Finite Element Analysis Program, USA
- [2] ASCE 41-06. (2006). Seismic Rehabilitation of Existing Buildings. American Society of Civil Engineers: Reston, VA.
- [3] Cakir, F. (2011), "Assessment of structural integrity and seismic retrofit of masonry bridges using micropiles", MSc., Thesis, Department of Civil, Architectural and Environmental Engineering, Graduate College of the Illinois Institute of Technology, Chicago, USA.
- [4] Cakir, F., Uysal, H. (2014). "Seismic performance of the historical masonry clock tower and influence of the adjacent walls". *Earthquakes and Structures*, 7(2), 217-231.
- [5] Cakir, F., Seker, B.S. (2015). "Structural performance of renovated masonry low bridge in Amasya, Turkey", *Earthquakes and Structures*, 8(6), 1387-1406
- [6] Cakir, F., Seker, B.S. and Dogangun, A. (2014). "Assessment of structural performance of historical Ishan Church with experimental tests and numerical modeling", *Gradevinar, J. Croatian Soc. Civ. Eng.*, 66(5), 433-443.
- [7] FEMA 274, (1997). NEHRP Commentary on the Guidelines for the Seismic Rehabilitation of Buildings. Federal Emergency Management Agency: USA.
- [8] FEMA 356, (2000). Prestandard and Commentary for the Seismic Rehabilitation of Buildings. Federal Emergency Management Agency: USA
- [9] KantarAtlas, (2018). <https://kantaratlasm.blogspot.com/2017/11/gebze-bridge.html?view=flipcard>
- [10] Meyer, P.K., (2006). "The impact of high frequency/low energy seismic waves on unreinforced masonry", M.Sc Thesis, Massachusetts Institute of Technology, Cambridge, USA
- [11] Sevim, B., Bayraktar A., Altunisik A.C., Atamturktur S. & Birinci F., (2011). "Assessment of nonlinear seismic performance of a restored historical arch bridge using ambient vibrations", *Nonlinear Dynamics* (2011) 63: 755–770
- [12] Şükür, R, (2008). <http://www.gazeteulus.com/yuzlerce-yillik-tarihi-miras-mimar-sinan-koprusu.html>
- [13] Ural, A., Oruç, Ş., Doğangün, A. & Tuluk Ö İ, (2008), "Turkish historical arch bridges and their deteriorations and failures", *Engineering Failure Analysis*, 15, 43–53.